7(2010) 413 – 422



Latin American Journal of Solids and Structures
www.lajss.org

Effects of abrasion on the penetration of ogival-nosed projectiles into concrete targets

Abstract

This paper investigates the effects of abrasion on the penetration of an ogival-nosed projectile into concrete targets. A numerical procedure is constructed based on an abrasion model which is proposed based upon the experimental observations and a forcing function. The forcing function is a polynomial of the normal velocity which approximates the response of target and can be determined either empirically or theoretically or numerically. The proposed numerical procedure is easy to implement and can be used to calculate the time-histories of projectile velocity, penetration depth, deceleration, mass loss and its nose shape. It is found that the model predictions are in good agreement with available test data in terms of mass loss, penetration depth and nose shape change of the projectile.

Keywords

ogival-nosed projectile, penetration, concrete, abrasion, numerical simulation.

H. M. Wen*, Y. Yang and T. He

CAS Key Laboratory for Mechanical Behavior and Design of Materials, University of Science and Technology of China, Hefei, Anhui 230027 – P. R. China

Received 7 Jun 2010;
In revised form 16 Nov 2010

* Author email: hmwen@ustc.edu.cn

1 INTRODUCTION

Some analytical or semi-analytical models have been developed to predict the penetration and perforation of targets struck normally by projectiles [3, 5, 12]. In these models, the target response is represented by a forcing function which applies to the projectile surface as pressure boundary conditions and could be determined using analytical or semi-empirical methods. For example, cavity expansion theory is used to derive the analytical forcing function equations [11, 12] in brittle or metallic targets and semi-empirical equations proposed by Wen [9, 10, 15, 16] are used for FRP laminates. These analytical or semi-analytical models can also be combined with FEA software to investigate the behaviour of a projectile in which the target response is represented by a forcing function as pressure boundary conditions [14]. This procedure is more efficient and accurate since there is no need to discretize the target and to consider complicated contact problem. However, abrasion and mass loss during penetration is always hard to be determined directly using these analytical or semi-analytical models even combining with FEA software.

Beissel and Johnson [1, 2] developed a computational model by assuming that the rate of mass loss on a projectile surface is proportional to the normal component of the sliding

velocity between the projectile and the target. By combining the model with full finite element analysis, the nose shape and mass loss of projectile can be simulated successfully to some extent. However, predicted projectile nose shapes are more extensive than experimental observations. More recently, Silling and Forrestal [13] proposed a new abrasion model in which the rate of mass loss is proportional to local sliding velocity. Thus, the projectile tip has minimum velocity and the model maximum abrasion toward the projectile shank rather than the nose tip. This model involves only axial forces and rigid-body velocities, and does not explicitly involve tangential traction and relative velocity between the projectile and target, which are difficult to measure or compute. This model has now been incorporated into CTH code, and an Eulerian hydrocode using the two-dimensional axisymmetric option in the code can be used to predict the nose shape and mass loss of the projectile.

In this paper, a numerical procedure is constructed based on an abrasion model which is proposed based upon the experimental observations and a forcing function. The forcing function is a polynomial of the normal velocity which approximates the response of target and can be determined either empirically or analytically. The projectile is assumed to be rigid and thus the motion of the projectile during penetration is controlled by Newton's second law. Numerical results are compared with some available experimental data and the influences of various parameters discussed.

2 PENETRATION MODELS WITH ABRASION

Silling and Forrestal [13] found that, when a projectile penetrates concrete targets, the mass loss can be written as

$$\frac{\Delta m}{m_0} = \frac{c_0 V_s^2}{2} \tag{1}$$

where V_s is initial velocity, Δm and m_0 are the mass loss and total mass before penetration and c_0 is an empirical constant which depends on the target material properties (the unconfined compression strengths, densities and maximum aggregate diameters of the concretes) and geometry of projectile (the projectile diameter, initial masses, nose shape). However, it can be seen from Eq. (1) that empirical constant c_0 is not a dimensionless parameter. It implies that the value of c_0 may be different when any parameter of the target or the projectile changes, which greatly limits the range of applicability of Eq. (1). In order to demonstrate the limitation of Eq. (1), test data from literature are plotted as $\Delta m/m_0$ versus V_s^2 in Fig. 1 where cases 1-4 are from [6], and cases 5-6 are from [7]. It is very clear from Fig. 1 that the data are rather scattered and the value of c_0 in Eq. (1) is obviously not a constant for which Mohs hardness for aggregates of concrete targets may be mainly responsible according to the study in reference [4].

In the present paper, a formula for the mass loss of a projectile penetrating concrete targets is derived by employing the principle of dimensional analysis together with the experimental observations. It is assumed here that the mass loss is a function of the relative strength of the

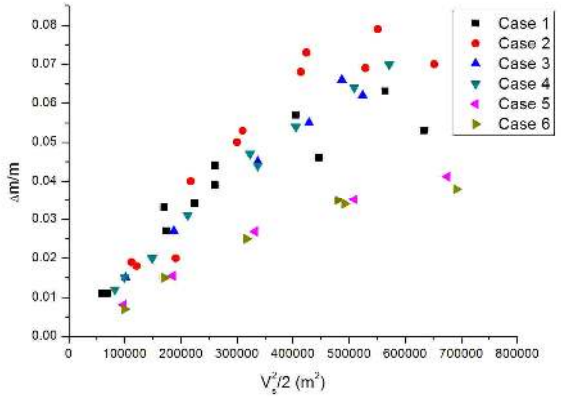

Figure 1 Relationship between $\Delta m/m_0$ and V_s^2.

target and projectile materials (Y_p/Y_t), the damage number ($\rho_t V_s^2/Y_t$), and the Mohs Hardness (Moh) which can be written in the following non-dimensional form

$$\frac{\Delta m}{m} = p\left(Moh \cdot \frac{Y_t}{Y_p}\left(\frac{\rho_t}{Y_t}\frac{V_s^2}{2}\right)\right)^q = p\left(Moh \cdot \frac{\rho_t}{2Y_p}V_s^2\right)^q \tag{2}$$

where Y_p and Y_t are the yield strength of projectile and target materials respectively, ρ_t is the density of target, Moh is the Mohs Hardness of aggregates, p and q are dimensionless empirical constants. It is seen from Fig. 2 that all the data collapse into one line and Eq. (2) with $p = 0.0162$ and $q = 0.805$ is in good correlation with the experimental data.

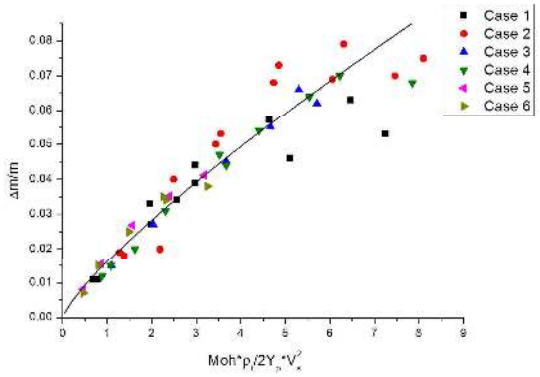

Figure 2 Variation of $\Delta m/m_0$ with Moh*$\rho_t V_s^2/2Y_p$.

Eq. (2) shows that the mass loss during penetration is a function of initial mass and initial velocity. Considering a moment during penetration, the current mass and velocity are m and V_z respectively. To calculate the mass loss after this moment, we can also use Eq. (2), namely

$$\frac{\Delta m}{m} = p\left(Moh \cdot \frac{\rho_t}{2Y_p} V_z^2\right)^q \tag{3}$$

Thus, at any given time, the incremental mass removal in any increment of time dt can be written as

$$\dot{m} = m \cdot p\left(Moh \cdot \frac{\rho_t}{2Y_p}\right)^q 2qV_z^{2q-1}\frac{dV_z}{dt} = 2pq\left(Moh \cdot \frac{\rho_t}{2Y_p}\right)^q V_z^{2q-1}F_z \tag{4}$$

whereF_z is the total axial force. The mass removal rate on unit area dA can be written as

$$d\dot{m} = -2pq\left(Moh \cdot \frac{\rho_t}{2Y_p}\right)^q V_z^{2q-1}\left(\sigma_n \sin\theta + \mu\sigma_n \cos\theta\right) dA \tag{5}$$

after taking into account the contribution of the friction to F_z. In Eq. (5) θ is defined as the angle between the tangential direction to the projectile surface and the axial direction of the projectile, μ is the friction coefficient, σ_n is normal stress to the projectile surface which is a forcing function approximating the target response. The forcing function can be expressed as a polynomial function of the expansion velocity of the target material and is determined either empirically or analytically [8].

Also, the mass loss rate can be expressed using abrasion velocity, v_a, the nodal velocity relative to projectile. This leads to [13]

$$d\dot{m} = -\rho_p v_a dA \tag{6}$$

Combining Eqs. (5), (6) and rearranging gives

$$v_a = \frac{2pq}{\rho_p}\left(Moh \cdot \frac{\rho_t}{2Y_p}\right)^q V_z^{2q-1}\sigma_n(\sin\theta + \mu\cos\theta) \tag{7}$$

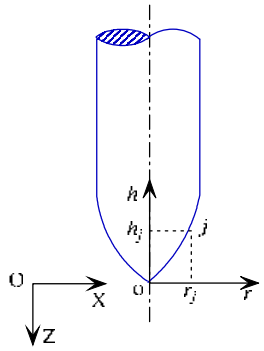

Figure 3 Schematic diagram showing the global and local coordinates for an ogival-nosed projectile.

Due to the complexity of the problem, analytical solution for this abrasion model is impractical. Instead, a numerical method is used to computer the mass loss and change of nose

shape. It is assumed that the whole penetration process can be divided into a number of steps, each with a small constant time increment Δt. Within every time increment, it is assumed that deceleration of a projectile is a constant. Fig. 3 shows schematically the global (XOZ) and local coordinates (roh) for the ogival-nosed projectile. The projectile penetrates the target with transient velocity V_z in global coordinate and the nodes on the nose surface move with the relative abrasion velocity v_a in local coordinate. Furthermore we assume that the number of increment along contour line of the projectile is j with the coordinate r_j and h_j and the angle between the tangential and axial direction is θ_j. From Newton's second law of motion, we have the following set of equations which can be obtained at every specified step i:

$$\Delta z = V_i \Delta t + \frac{1}{2} a_i \Delta t^2 \qquad \text{(displacement increment)} \tag{8}$$

$$z_{i+1} = z_i + \Delta z \qquad \text{(displacement)} \tag{9}$$

$$V_z^{i+1} = V_z^i + a_i \Delta t \qquad \text{(velocity)} \tag{10}$$

$$V_{n\,j+1}^{i+1} = V_z^{i+1} \sin\left[\frac{1}{2}\left(\theta_j^i + \theta_{j+1}^i\right)\right] \qquad \text{(normal velocity)} \tag{11}$$

$$V_{t\,j+1}^{i+1} = V_z^{i+1} \cos\left[\frac{1}{2}\left(\theta_j^i + \theta_{j+1}^i\right)\right] \qquad \text{(tangential velocity)} \tag{12}$$

$$v_{a\,j+1}^{i+1} = \frac{2pq}{\rho_p}\left(Moh \cdot \frac{\rho_t}{2Y_p}\right)^q (V_z^{i+1})^{2q-2} \sigma_{n\,j+1}^{i+1} (V_{n\,j+1}^{i+1} + \mu V_{t\,j+1}^{i+1}) \qquad \text{(abrasion velocity)} \tag{13}$$

$$r_{j+1}^{i+1} = r_{j+1}^i - v_{a\,j+1}^{i+1} \cos\left[\frac{1}{2}\left(\theta_j^i + \theta_{j+1}^i\right)\right] \Delta t \qquad \text{(nodal radius)} \tag{14}$$

$$h_{j+1}^{i+1} = h_{j+1}^i + v_{a\,j+1}^{i+1} \sin\left[\frac{1}{2}\left(\theta_j^i + \theta_{j+1}^i\right)\right] \Delta t \qquad \text{(nodal height)} \tag{15}$$

$$\theta_j^i = \arctan\left[\left(r_{j+1}^{i+1} - r_j^{i+1}\right) / \left(h_{j+1}^{i+1} - h_{j+1}^i\right)\right] \qquad \text{(tangential angel)} \tag{16}$$

$$\sigma_{n\,j+1}^{i+1} = A + B V_{n\,j+1}^{i+1} + C\left(V_{n\,j+1}^{i+1}\right)^2 \qquad \text{(forcing function)} \tag{17}$$

$$m_{i+1} = \sum_j \frac{\pi}{2}\left(r_{j+1}^{i+1} + r_j^{i+1}\right)\left(h_{j+1}^{i+1} - h_j^{i+1}\right)\rho_p \qquad \text{(mass)} \tag{18}$$

$$df_{z\,j+1}^{i+1} = \frac{\pi}{2}\left(\sigma_{j+1}^{i+1} + \sigma_j^{i+1}\right)\left(\left[\left(r_{j+1}^{i+1}\right)^2 - \left(r_j^{i+1}\right)^2\right] + 2\mu r_j^{i+1}\left(h_{j+1}^{i+1} - h_j^{i+1}\right)\right) \qquad \text{(element axial force)} \tag{19}$$

$$f_z^{i+1} = \sum_j df_{z\,j}^{\,i+1} \qquad \text{(total axial force)} \tag{20}$$

$$a_{i+1} = f_z^{i+1}/m_{i+1} \qquad \text{(total acceleration)} \tag{21}$$

$$t_{i+1} = t_i + \Delta t \tag{22}$$

Given initial conditions: $t_0 = 0$, $a_0 = 0$, $V_z^0 = V_s$ and $z_0 = 0$, the time-histories can be calculated by repeating Eqs. (8)- (22) and then the abrasion effects such as the depth of penetration, the mass loss rate, the change of projectile nose shapes can also be calculated. MATLAB is used to solve the problems.

3 COMPARISONS AND DISCUSSION

Comparisons are made between the present numerical results and some experimental data for concrete targets with quartz aggregates (case 3 of [13]) and limestone aggregates (case 5 of [7]). In case 3, the density of concrete is 2300kg/m^3, uniaxial unconfined compression strength Y_t = 63MPa and the Mohs Hardness Moh = 7 for the quartz aggregates. The projectile material is 4340 Rc45 steel with yield strength Y_p = 1481MPa and ρ_p = 7810kg/m^3. The projectile diameter d = 20.3mm, projectile mass m = 0.478kg, CRH = 3 and the ratio of length to diameter l/d = 10. In the calculation, the effect of friction is ignored, i.e. $\mu = 0$ (friction is neglected for two reasons, one reason is that frictional coefficient is velocity dependent and is difficult to determine; the other is that a constant frictional coefficient does not give a consistent predictions for the depth of penetration especially at high impact velocities as projectile nose shape becomes blunter due to abrasion). Forrestal's semi-empirical equation [5] is used to calculate the coefficient of forcing function, σ_n. Since the uniaxial unconfined compression strength is equal to 63MPa, from Forrestal's semi-empirical equation, we can get A = 540MPa, $B = 0$, C = 2300kg/m^3. In case 5, the density of concrete is 2320kg/m^3, uniaxial unconfined compression strength Y_t = 58.4MPa and the Mohs Hardness Moh = 3 for the limestone aggregates. From Forrestal's semi-empirical equation, we can get A = 530MPa, $B = 0$, C = 2320kg/m^3. The projectiles used in case 5 penetration tests are the same as those employed in case 3 penetration tests. It is easy to implement Eqs. (8)-(22) into MATLAB and the penetration and deformation of the projectiles can be calculated which are presented in the following.

3.1 Projectile mass loss

Figs. 4(a) and 4(b) show comparisons of the present numerical results with the experimental data for case 3 of [13] and case 5 of [7]. Also shown in these two figures are the results of the empirical equations (Eq. (1) and Eq. (2)). It has to be mentioned here that for case 3 and case 5 different values of c_0 are used in the calculation of Eq. (1) (i.e. $c_0 = 0.13$ for case 3 and c_0

= 0.067 for case 5). It is seen from Fig. 4 that the numerical results are almost identical with Eq. (2) which are found to be in better agreement with the test data compared to Eq. (1).

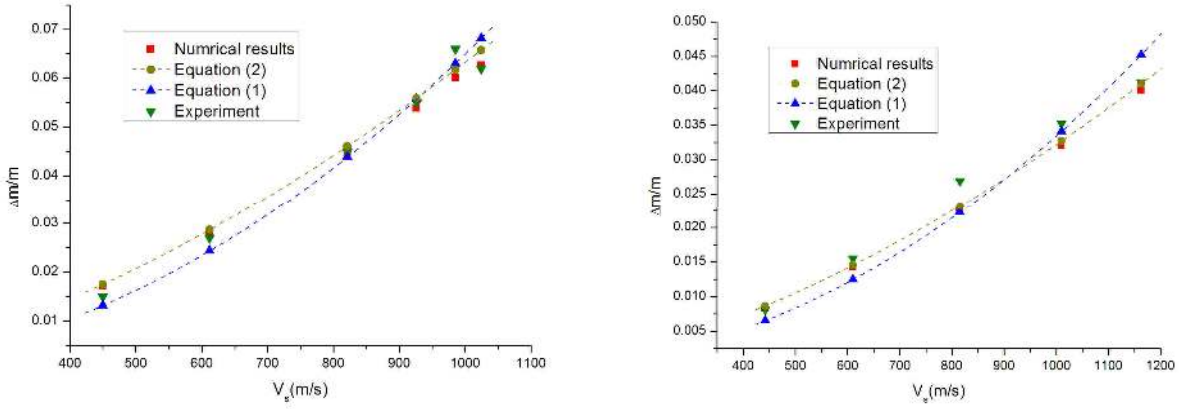

(a) (b)

Figure 4 Comparisons of various model predictions with experimental data for projectile mass loss. (a) case 3 of [12], (b) case 5 of [14].

3.2 Depth of penetration

Figs. 5(a) and 5(b) show variation of penetration depth with impact velocity for case 3 of [13] and case 5 of [7], respectively. Also shown in the figures are the predictions from our present numerical procedure with or without abrasion. It is evident from Fig. 5 that the present numerical results are in good agreement with the experimental data. It is also evident from Fig. 5 that the effect of abrasion on the depth of penetration increases with increasing impact velocity. For relatively low impact velocities the effect on penetration depth is negligibly small and for higher impact velocities the effect becomes large but still within a few percent for the highest impact velocity examined.

3.3 Change of nose shape

Figs. 7 and 8 show comparisons of the present numerically predicted nose shapes with the experimental observations for ogival-nosed projectiles penetrating concrete targets at various velocities [7, 13]. Broken and red solid lines show respectively the original nose shapes and the deformed shapes computed from the present numerical procedure whilst the experimentally observed nose shapes are shown as the shadow. It is clear from Figs. 7 and 8 that the proposed numerical procedure can be used to compute the deformed configuration of a projectile nose though there are still some differences between the predicted nose shape and the experimental observation. There are two factors which may be responsible for the difference. First, the procedure cannot handle the singularity well at the projectile tip; second, there may be melting

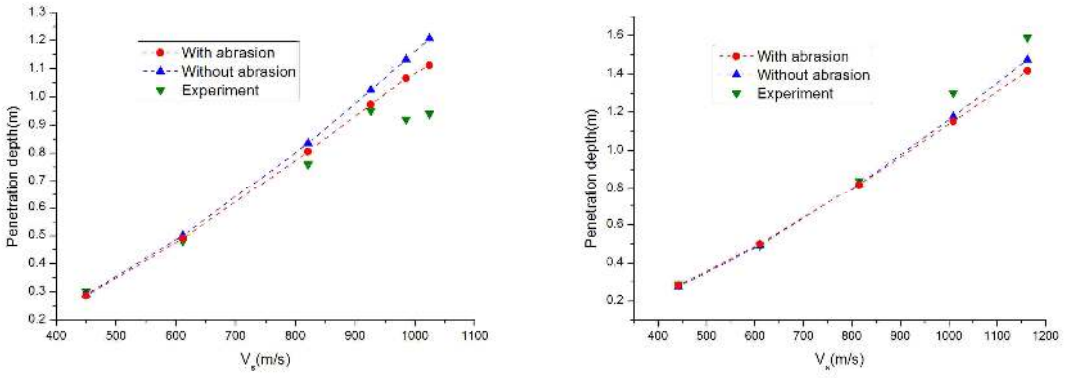

(a) case 3 of [13] (b) case 5 of [7]

Figure 5 Comparison of the present numerical results with the test data..



(a) $V_s = 612\text{m/s}$ (b) $V_s = 985\text{m/s}$

Figure 6 Comparison of the numerically predicted nose shape with the experimental observations for case 3 of [13]. _ _ _ shows the original nose shape of the projectile, ____ shows the numerically predicted nose shape of the projectile.

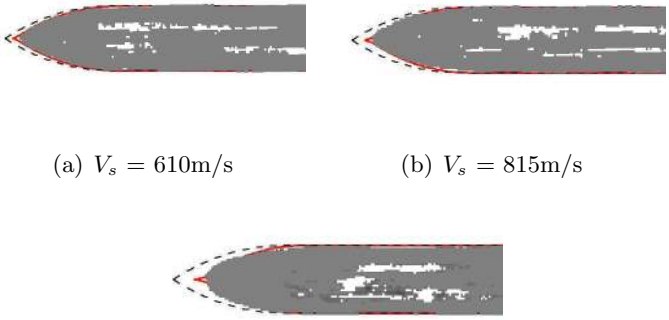

(a) $V_s = 610\text{m/s}$ (b) $V_s = 815\text{m/s}$

(c) $V_s = 1162\text{m/s}$

Figure 7 Comparison of the numerically predicted nose shape with the experimental observations for case 5 of [7]. _ _ _ shows the original nose shape of the projectile, ____ shows the numerically predicted nose shape of the projectile.

or fracture of the head in the process of penetration as can be seen from the photographs that the projectile noses became irregular after penetrating concrete targets at high speeds, which cannot be described by the present finite difference procedure. All these points indicate that there is still room for further improvement of the present finite difference procedure.

4 CONCLUSIONS

The effects of abrasion on the penetration of an ogival-nosed projectile into concrete targets have been examined in the paper. Based on the experimental observations and a forcing function an abrasion model was first proposed and the used to construct a numerical procedure. The forcing function is a polynomial of the normal velocity which approximates the response of target and can be determined either empirically or theoretically or numerically. The proposed numerical procedure is easy to implement and can be used to calculate the time-histories of projectile velocity, penetration depth, deceleration, mass loss and its nose shape. It is found that the model predictions are in good agreement with available test data in terms of mass loss, penetration depth. It is also found that the numerical procedure can be employed to compute the nose shape change of a projectile penetrating concrete targets at relatively low velocities and that at higher impact velocities it predicts less well the projectile nose shape change as only abrasion is taken into account in the procedure.

References

[1] S. R. Beissel and G. R. Johnson. An abrasion algorithm for projectile mass loss during penetration. *Int J Impt Engng*, 24:103–116, 2000.

[2] S. R. Beissel and G. R. Johnson. A three-dimensional abrasion algorithm for projectile mass loss during penetration. *Int J Impt Engng*, 27:771–789, 2002.

[3] G. Ben-Dor, A. Dubinsky, and T. Elperin. Ballistic impact: recent advances in analytical modeling of plate penetration dynamics – a review. *Applied Mechanics Reviews*, 58:355–371, 2005.

[4] X. W. Chen and S. Q. Yang. Modeling on mass abrasion of kinetic energy penetrator. *Chinese Journal of Theoretical and Applied Mechanics*, 5:739–747, 2009.

[5] M. J. Forrestal, B. S. Altman, J. D. Cargile, and S. J. Hanchak. An empirical equation for penetration of ogive-nose projectiles into concrete target. *Int J Impact Engng*, 15:395–405, 1994.

[6] M. J. Forrestal, D. J. Frew, S. J. Hanchak, and N. S. Brar. Penetration of grout and concrete targets with ogive-nose steel projectiles. *Int J Impact Engng*, 18(5):465–476, 1996.

[7] D. J. Frew, S. J. Hanchak, M. L. Green, and M. J. Forrestal. Penetration of concrete targets with ogive-nose steel rods. *Int J Impt Engng*, 21(6):489–497, 1998.

[8] T. He and H. M. Wen. Determination of the analytical forcing function of target response and its applications in penetration mechanics. *Journal of University of Science and Technology of China*, 10:101–113, 2007.

[9] T. He, H. M. Wen, and Y. Qin. Penetration and perforation of FRP laminates struck transversely by conical-nosed projectiles. *Compos Struct*, 81(2):243–252, 2007.

[10] T. He, H. M. Wen, and Y. Qin. Finite Element Analysis to predict penetration and perforation of thick FRP laminates struck by projectiles. *Int J Impt Engng*, 35(1):27–36, 2008.

[11] R. Hill. *The mathematical theory of plasticity*. Oxford University Press, London, 1950.

[12] Q. M. Li, S. R. Reid, H. M. Wen, and A. R. Telford. Local impact effects of hard missiles on concrete targets. *Int J Impt Engng*, 32(1-4):224–284, 2006.

[13] S. A. Silling and M. J. Forrestal. Mass loss from abrasion on ogive-nose steel projectiles that penetrate concrete targets. *Int J Impt Engng*, 34(11):1814–1820, 2007.

[14] T. L. Warren and M. R. Tabbara. Simulations of the penetration of 6061-T6511 aluminum targets by spherical-nosed VAR4340 steel projectiles. *Int J Solids Struct*, 37(44):4419–4435, 2000.

[15] H. M. Wen. Predicting the penetration and perforation of FRP laminates struck normally by projectiles with different nose shapes. *Compos Struct*, 49(3):321–329, 2000.

[16] H. M. Wen. Penetration and perforation of thick FRP laminates. *Compos Sci Technol*, 61(8):1163–1172, 2001.